MISSOURI
S&T

Missouri University of Science and Technology

Scholars' Mine

Electrical and Computer Engineering Faculty Research & Creative Works

Electrical and Computer Engineering

01 Feb 2008

Fault-Tolerant Optimal Neurocontrol for a Static Synchronous Series Compensator Connected to a Power Network

Wei Qiao

Ronald G. Harley

Ganesh K. Venayagamoorthy
Missouri University of Science and Technology

Follow this and additional works at: https://scholarsmine.mst.edu/ele_comeng_facwork

Part of the Electrical and Computer Engineering Commons

Recommended Citation

Fault-Tolerant Optimal Neurocontrol for a Static Synchronous Series Compensator Connected to a Power Network

Wei Qiao, *Student Member, IEEE*, Ronald G. Harley, *Fellow, IEEE*,
and Ganesh Kumar Venayagamoorthy, *Senior Member, IEEE*

Abstract—This paper proposes a novel fault-tolerant optimal neurocontrol scheme (FTONC) for a static synchronous series compensator (SSSC) connected to a multimachine benchmark power system. The dual heuristic programming technique and radial basis function neural networks are used to design a nonlinear optimal neurocontroller (NONC) for the external control of the SSSC. Compared to the conventional external linear controller, the NONC improves the damping performance of the SSSC. The internal control of the SSSC is achieved by a conventional linear controller. A sensor evaluation and (missing sensor) restoration scheme (SERS) is designed by using the autoassociative neural networks and particle swarm optimization. This SERS provides a set of fault-tolerant measurements to the SSSC controllers, and therefore, guarantees a fault-tolerant control for the SSSC. The proposed FTONC is verified by simulation studies in the PSCAD/EMTDC environment.

Index Terms—Dual heuristic programming (DHP), fault-tolerant optimal neurocontrol, missing sensor restoration (MSR), particle swarm optimization (PSO), radial basis funtion network, static synchronous series compensator (SSSC).

I. INTRODUCTION

THE STATIC synchronous series compensator (SSSC) [1], using a voltage source converter to inject a controllable voltage in quadrature with the line current of a power network, belongs to the family of series flexible ac transmission system (FACTS) devices. Such a device is able to rapidly provide both capacitive and inductive impedance compensation independent of the power line current. Moreover, an SSSC with a suitably designed external damping controller [2]–[4] can also be used to improve the damping of the low-frequency power oscillations in a power network. These features make the SSSC an attractive FACTS device for power flow control, power oscillation damping, and improving transient stability.

In [5], Rigby and Harley reported an internal control scheme for an SSSC based on a voltage-source inverter. They extended this research by proposing a power oscillation damping scheme achieved by a suitably designed conventional external linear controller (CONVEC) to the SSSC [2].

In a previous work [4], the present authors proposed an indirect adaptive neurocontroller for the external control of an SSSC. This neurocontroller has the superior damping performance over the CONVEC. However, the indirect adaptive control approach cannot avoid the possibility of instability during steady state at various operating conditions [6]. To overcome the issue of instability and provide robustness for the controller, the adaptive critic designs (ACDs) technique [7], [8] for optimal nonlinear control has been recently developed and applied to controlling nonlinear plants in power systems [3], [6], [9].

Control of nonlinear systems relies on the availability and the quality of sensor measurements. Measurements are inevitably subjected to faults that can be caused by sensor failure, broken or bad connections, bad communication, or malfunction of some hardware or software (these are referred to as missing sensor measurements in this paper). If some sensors fail to provide the correct information, the controllers cannot guarantee the correct control behavior for the system based on the faulty input data. Therefore, fault-tolerance [10] is an essential requirement for system control.

This paper proposes a fault-tolerant optimal neurocontrol scheme (FTONC) for an SSSC connected to a multimachine benchmark power system. The dual heuristic programming (DHP) [7], [8] technique and radial basis function neural networks (RBFNNs) [4] are used to design the nonlinear optimal neurocontroller (NONC) for the SSSC external control. This NONC provides improved damping performance over the CONVEC used by the SSSC. The internal control of the SSSC is still achieved by a conventional linear controller. A sensor evaluation and (missing sensor) restoration scheme (SERS) is designed by using the autoassociative neural networks (autoencoder) [11], [12] and particle swarm optimization (PSO) [13], [14]. This SERS provides a set of fault-tolerant measurements to the internal and external controllers of the SSSC, and therefore, guarantees a fault-tolerant control for the SSSC.
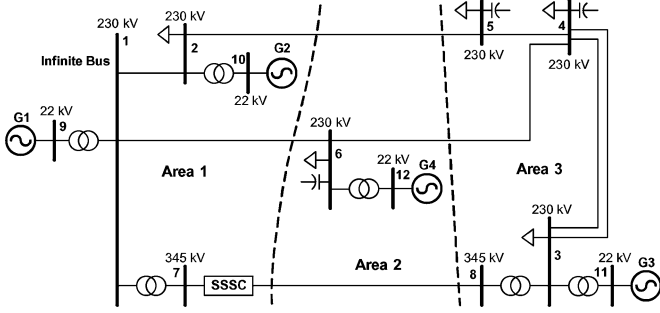
Fig. 1. Single-line diagram of the 12-bus power system with an SSSC.

II. POWER SYSTEM MODEL

The four-machine 12-bus benchmark power system in Fig. 1 was proposed [15] as a platform system for studying FACTS device applications. The system consists of six 230 kV busses, two 345 kV busses, and four 22 kV busses. It covers three geographical areas. Area 1 is predominantly a generation area with most of its generation coming from hydro power (G1 and G2). Area 2, located between the main generation area (area 1) and the main load center (area 3), has some hydro generation available (G4) but is insufficient to meet local demand. Area 3, situated about 500 km from area 1, is a load center with some thermal generation (G3) available. Furthermore, since the generation unit in area 2 has limited energy available, the system demand must often be satisfied through transmission. The transmission system consists of 230 kV transmission lines except for one 345 kV link between areas 1 and 3 (between busses 7 and 8). Areas 2 and 3 have switched shunt capacitors to support the voltage. Power flow studies on this 12-bus system [15] reveal that in the event of a loss of generation in area 3, or a loss of the transmission line between busses 4 and 5, line 1–6 is overloaded while the transmission capacity of the parallel path through the 345 kV transmission line 7–8 is underutilized. This congestion can be relieved by placing an SSSC on line 7–8. Moreover, with a suitably designed external damping controller, the SSSC can improve power oscillation damping of the system during various transient disturbances.

In this paper, G1 is represented as a three-phase infinite source, while the other three generators are modeled in detail, with the exciter and turbine governor dynamics taken into account.

III. SSSC AND ITS CONVENTIONAL LINEAR CONTROLLERS

The schematic diagram of the internal control scheme for the SSSC is shown in Fig. 2. The main objectives of this internal control are to ensure that the injected controllable voltage $v_{c,abc}$ (by injecting a desired compensating reactance X_C^*) at the ac terminals of the inverter, remains in quadrature with the transmission line current, as well as keeping the dc terminal voltage of the inverter constant at steady state. A detailed description of the internal controller is given in [5].

The objective of the CONVEC (Fig. 3) is to damp the transient power oscillations of the system. This external controller is able to rapidly change the compensating reactance X_C injected
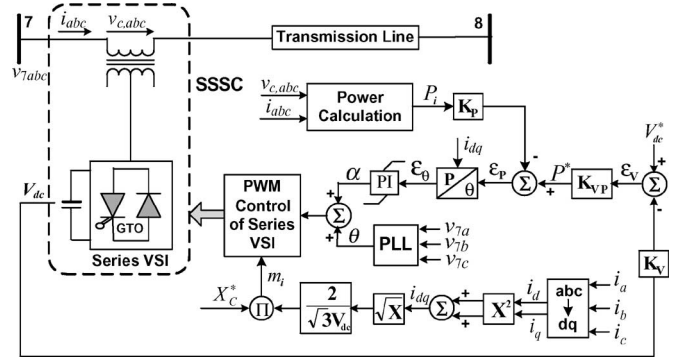

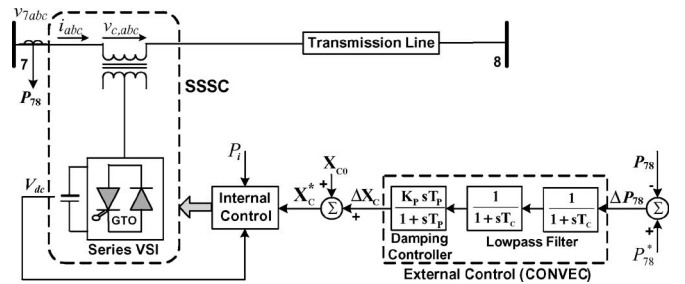Fig. 2. Schematic diagram of the SSSC internal controller.

Fig. 3. Schematic diagram of the SSSC external damping controller.

by the SSSC, thus providing supplementary damping during transient power swings [2]–[4]. In a practical controller, it is usually desirable to choose a local signal. In this paper, the active power deviation ΔP_{78} on line 7–8 (measured at bus 7 side), is used as the input signal to the CONVEC. In Fig. 3, ΔP_{78} is passed through two first-order low-pass filters and a damping controller (consisting of a proportional damping gain K_P and a washout filter) [2]–[4] to form a supplementary control signal ΔX_C, which is then added to a steady-state fixed set point value X_{C0} to form the total commanded value of compensating reactance X_C^* at the input of the SSSC internal controller. The washout filter is a high-pass filter that removes the dc offset, and without it the steady changes in active power P_{78} would modify the value of compensating reactance. The use of two low-pass filters is based on two reasons: 1) filtering the electrical noise in the measurements and 2) phase compensation to ensure that the variations in compensating reactance are correctly phased with respect to the transient power oscillations in order to provide supplementary damping. Values of the CONVEC parameters $K_P = 10$, $T_C = 0.5$ s, and $T_P = 0.1$ s are used for several case studies in Section VI.

IV. NONLINEAR OPTIMAL EXTERNAL NEUROCONTROLLER

In this section, a NONC is designed by applying the DHP method and the RBFNNs. This NONC is used to replace the CONVEC in Fig. 3 for the external damping control of the SSSC, as shown in Fig. 4.
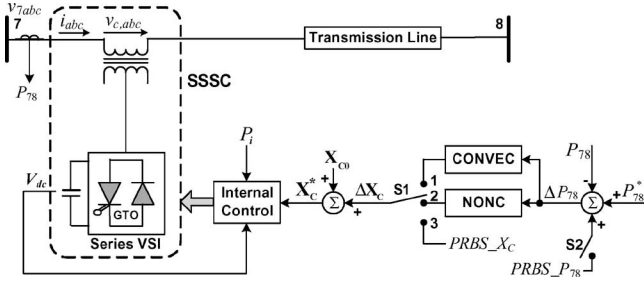
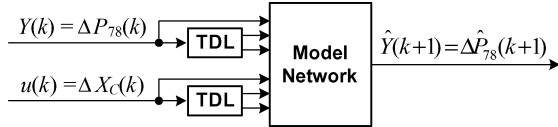Fig. 4.   Schematic diagram of the SSSC with internal and external controllers.

Fig. 5.   Structure of the model network. TDL means time delay lock.

Fig. 6.   Identification results by the model network.

A. Adaptive Critic Designs and Dual Heuristic Programming

Adaptive critic designs, proposed by Werbos [7], is a neural network-based optimization and control technique that solves the classical nonlinear optimal control problems by combining concepts of *reinforcement learning* and *approximate dynamic programming*.

The DHP, belonging to the family of the ACDs, requires three neural networks for its implementation, one for the model, one for the critic, and one for the action network [7]–[9]. The model network is used to identify the input–output dynamics of the plant. The critic network estimates the derivatives of the function J (cost-to-go function in the Bellman equation of dynamic programming) with respect to the states of the plant Y, and J is given by

$$J(k) = \sum_{q=0}^{\infty} \gamma^q U(k+q) \qquad (1)$$

where $U(\cdot)$ is the utility function or one-stage cost (user-defined function) and γ is a discount factor for finite horizon problems $(0 < \gamma < 1)$. The ACD method determines optimal control laws for a system by successively adapting the critic and action networks. The adaptation process starts with a nonoptimal control by the action network; the critic network then guides the action network toward the optimal solution at each successive adaptation. During the adaptations, neither of the networks needs any information of the desired control trajectory, only the desired cost needs to be known.

B. Design of the Model Network

The model network is a three-layer RBFNN [4] with 15 hidden neurons. The plant input $u = \Delta X_C$ and output $Y = \Delta P_{78}$ at time k, $k-1$, and $k-2$ are fed into the model network to estimate the plant output $\hat{Y} = \Delta \hat{P}_{78}$ at time $k+1$, as shown in Fig. 5. The sampling period for the RBFNN implementation is 10 ms.

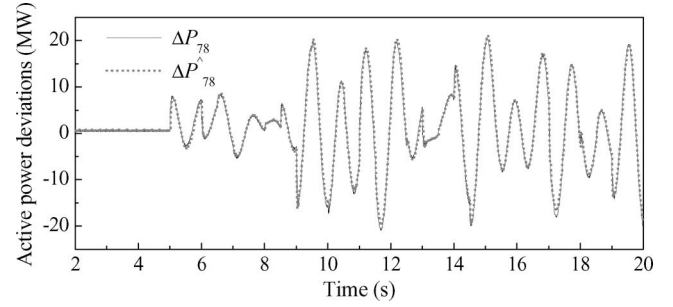The model network is trained offline using a suitably selected training data set collected from two sets of training. The first set is called *forced training*, in which the plant is perturbed by injected small pseudorandom binary signals (PRBS) (with S1 in position 3 in Fig. 4), given by

$$\text{PRBS}\_X_C(k) = 0.1|X_{C0}|[r0(k) + r1(k) + r2(k)]/3 \qquad (2)$$

where $r0$, $r1$, and $r2$ are uniformly distributed random numbers in $[-1, 1]$ with frequencies 0.5, 1, and 2 Hz, respectively. The second set is called *natural training*, in which the PRBS is removed (with S1 in position 1 in Fig. 4) and the system is exposed to natural disturbances and faults in the power network. The forced training and natural training are carried out at several different operating points to form the training data set, given by

$$\underline{A} = \{\underline{X}, \underline{Y}\} = \left\{ \bigcup_{i=1}^{m} \underline{A}_{Fi}, \bigcup_{i=1}^{m} \bigcup_{j=1}^{n} \underline{A}_{Nij} \right\} \qquad (3)$$

where $\underline{A}$ is the entire training data set selected from m operating points; $\underline{X}$ and $\underline{Y}$ are the input and output data sets of the model network, respectively; $\underline{A}_{Fi}$ is the subset collected from the forced training at the operating point i; $\underline{A}_{Nij}$ is the subset collected from the natural training caused by the jth natural disturbance event at the operating point i. The selected training data set ensures that the model network can track the system dynamics over a wide operating range. After determining the training data set, the weights of the model network are then calculated by singular value decomposition (SVD) [16] method.

After training has been completed, the PRBS defined by (2) is applied to the system in Fig. 4 from $t = 5$ s at an operating point where the model network has specifically not been trained. Fig. 6 shows the actual plant output ΔP_{78} and the estimated plant output $\Delta \hat{P}_{78}$ from the model network. The model network tracks the plant dynamics with good precision, therefore proving that the model network has learned the plant dynamics globally during the training stage.

C. Design of the Critic Network

The critic network is a three-layer RBFNN with 12 hidden neurons. The inputs to the critic network are the estimated plant output $\hat{Y} = \Delta \hat{P}_{78}$ (from the model network) and its two time-delayed values. The output of the critic network is the derivative $\lambda = \partial J / \partial \hat{Y}$ of the function J in (1) with respect to the estimated plant output $\hat{Y}$, as shown in Fig. 7.
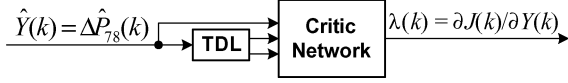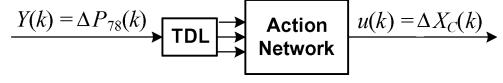
Fig. 7.   Structure of the critic network

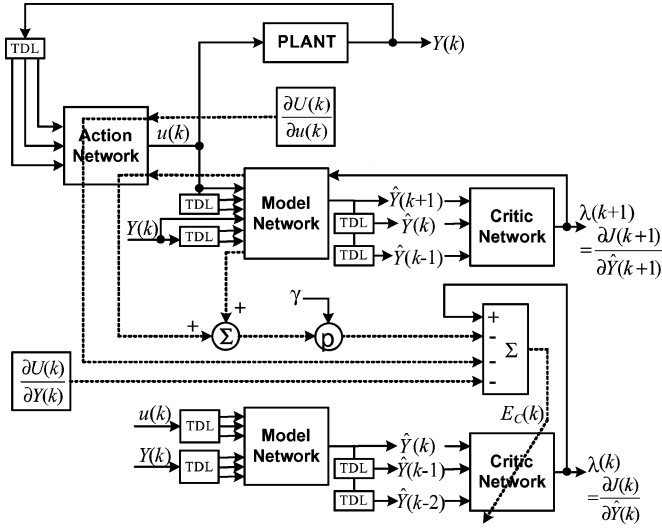Fig. 9.   Structure of the action network.

Fig. 8.   Adaptation of the critic network in the DHP.

Fig. 10.   Adaptation of the action network in the DHP.

The output weights of the critic network are updated by

$$\Delta W_C(k) = -\eta_C E_C^T(k) \frac{\partial \lambda[\hat{Y}(k)]}{\partial W_C(k)}$$

$$= -\eta_C E_C^T(k) \frac{\partial^2 J[\hat{Y}(k)]}{\partial \hat{Y}(k) \partial W_C(k)} \qquad (9)$$

where η_C is a positive learning gain.

D. Design of the Action Network

The action network (Fig. 9) is a three-layer RBFNN with 12 hidden neurons. The inputs to the action network are the plant output $Y = \Delta P_{78}$, at time $k-1$, $k-2$, and $k-3$. The output of the action network is the plant input $u = \Delta X_C$, at time k.

The adaptation of the action network, as shown in Fig. 10, is achieved by propagating $\lambda(k+1)$ back through the model to the action network [8]. The objective of such adaptation is to find out the optimal control trajectory u^* in order to minimize the cost-to-go function J over time, given by

$$u^*(k) = \arg \min_u[J(k)] = \arg \min_u[U(k) + \gamma J(k+1)] \quad (10)$$

which is equivalent to achieving the objective

$$\frac{\partial U(k)}{\partial u(k)} + \gamma \frac{\partial J(k+1)}{\partial u(k)} = 0 \qquad \forall k. \qquad (11)$$

The output weights of the action network are then updated by

$$\Delta W_A(k) = -\eta_A \left[\frac{\partial U(k)}{\partial u(k)} + \gamma \frac{\partial J(k+1)}{\partial u(k)} \right]^T \frac{\partial u(k)}{\partial W_A(k)}. \qquad (12)$$

E. Overall Training Procedure

The training procedure to implement the DHP algorithm consists of two training stages: one for the model network and the other for the critic/action networks. The model network is firstly trained offline to learn the plant dynamics before training the critic and action networks, as described in Section IV-B. Once the weights of the model network have converged, they are fixed during the training of the critic and action networks.

The critic network learns to minimize the following error measure over time [8]:

$$\|E_C\| = \sum_k E_C^T(k) E_C(k) \qquad (4)$$

where

$$E_C(k) = \frac{\partial J[\hat{Y}(k)]}{\partial \hat{Y}(k)} - \gamma \frac{\partial J[\hat{Y}(k+1)]}{\partial Y(k)} - \frac{\partial U(k)}{\partial Y(k)}. \qquad (5)$$

The utility function is defined as

$$U(k) = \tfrac{1}{2}\left[\Delta P_{78}^2(k) + 0.5\Delta P_{78}^2(k-1) + 0.1\Delta P_{78}^2(k-2)\right]. \qquad (6)$$

In the DHP, application of the chain rule for derivatives yields

$$\frac{\partial J[\hat{Y}(k+1)]}{\partial Y(k)} = \lambda(k+1)\left[\frac{\partial \hat{Y}(k+1)}{\partial Y(k)} + \frac{\partial \hat{Y}(k+1)}{\partial u(k)}\frac{\partial u(k)}{\partial Y(k)}\right] \qquad (7)$$

$$\frac{\partial U(k)}{\partial Y(k)} = \frac{\partial U(k)}{\partial Y(k)} + \frac{\partial U(k)}{\partial u(k)}\frac{\partial u(k)}{\partial Y(k)} \qquad (8)$$

where $\lambda(k+1) = \partial J[\hat{Y}(k+1)]/\partial \hat{Y}(k+1)$. Generally, two critic networks are required in the DHP to estimate $\partial J/\partial \hat{Y}$ arising from the present state $\hat{Y}(k)$ and the future state $\hat{Y}(k+1)$. The adaptation of the critic network in the DHP takes into account all relevant pathways of backpropagation as shown in Fig. 8.
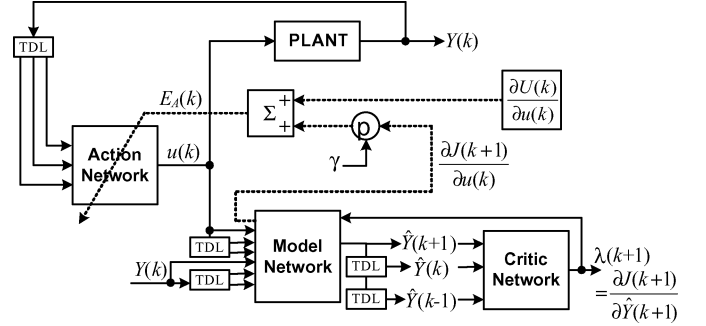
The training stage of the critic/action networks consists of two separate training cycles: one for the critic and the other for the action. The action network is firstly pretrained to learn the dynamics of the CONVEC. This ensures that the whole system, consisting of the NONC and the plant, remains stable. During the action's pretraining, the plant is controlled by the CONVEC (with S1 in position 1 in Fig. 4) and disturbed by injecting small PRBS (with S2 closed in Fig. 4) to P_{78}^*, given by

$$\text{PRBS}\_P_{78}(k) = 0.05|P_{78}^*|[r0(k) + r1(k) + r2(k)]/3. \quad (13)$$

Once the action's pretraining is over, S1 switches to position 2 and the plant is controlled by the NONC. Then, the action's weights are fixed, and the critic network is trained by the procedure in Fig. 8 until the error in (4) becomes acceptably small. Then, the critic's weights are fixed, and the action network is trained further by the procedure in Fig. 10. This process of training the critic/action networks is repeated one after the other until the error (11) becomes as small as possible. Once the critic and action networks' weights have converged, the action network with the fixed weights is used to control the plant during the real-time operation.

V. FAULT-TOLERANT CONTROL SCHEME

The operation and control of the SSSC (Figs. 2 and 3) rely on the availability and quality of four sets of sensor measurements: the three-phase currents i_{abc} of line 7–8, the three-phase voltages v_{7abc} of bus 7, the injected three-phase voltages $v_{c,abc}$ at the SSSC, and the dc-link voltage V_{dc}. Other variables, such as P_i and P_{78}, are calculated from these measured variables. In this section, a fault-tolerant control scheme is designed for both internal and external control of the SSSC. This control scheme provides fault tolerance to any set of major sensors (i_{abc}, v_{7abc}, v_{cabc}, and V_{dc}) faults based on two reasonable assumptions: 1) there is no multiple sets of sensors missing and 2) the power system operates under three-phase balanced condition at the transmission level.

A. Overall Structure of the Fault-Tolerant Control Scheme

Fig. 11 shows the overall structure of the proposed FTONC scheme for the SSSC. It consists of an internal controller, a NONC, and an SERS. The four sets of sensor data used by the SSSC internal and external controllers are fed into the SERS, which evaluates the integrity of these sensor data. If the SERS identifies that one or more sensors are missing, it is responsible for restoring all missing sensors. The output variables of the SERS with a subscript R represent the restored missing sensor data, while the output variables with a subscript H represent the healthy sensor data. If there is no sensor missing, the outputs with a subscript H are exactly the same as the corresponding inputs (e.g., $i_H = i_{abc}$). Now the active power P_{78} used by the NONC is calculated from $[i_H, i_R]$ and $[v_{7H}, v_{7R}]$, and the active power P_i used by the internal controller is calculated from $[i_H, i_R]$ and $[v_{cH}, v_{cR}]$. Other sensor data used by the internal controller consist of $Z_H = [i_H, v_{7H}, V_{dcH}]$ and $Z_R = [i_R, v_{7R}, V_{dcR}]$. The SERS provides a set of complete sensor data to the SSSC controllers even when some sensors are
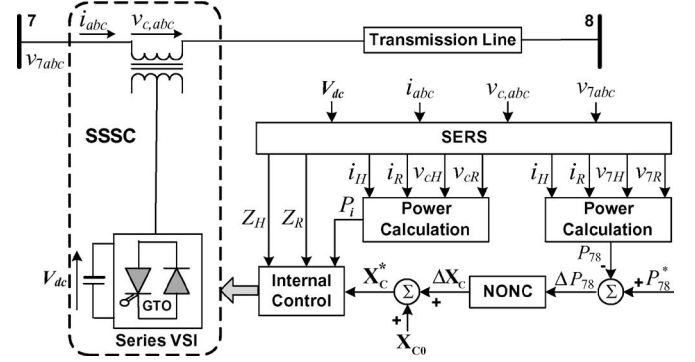
Fig. 11. Overall structure of the FTONC.
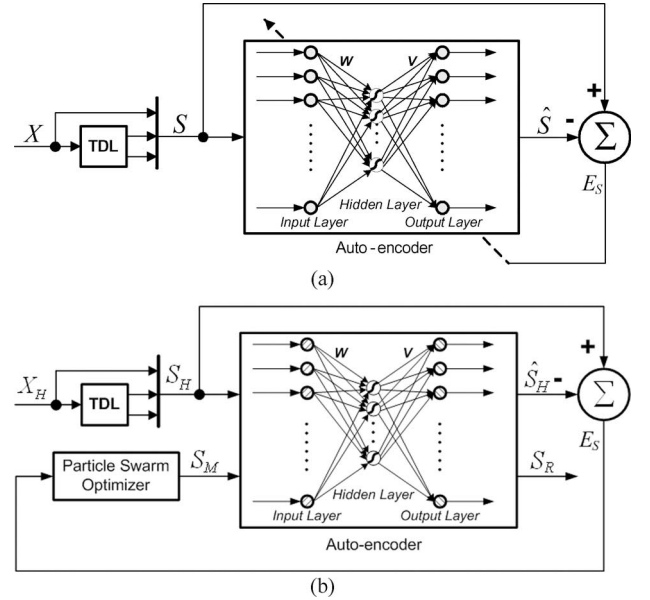
Fig. 12. Overall structure of the MSR. (a) Training of the autoencoder. (b) Online restoration of missing sensor data.

missing, and therefore, guarantees a fault-tolerant control for the SSSC.

B. Missing Sensor Restoration (MSR) Algorithm

For many systems, certain degrees of redundancy are present among the data collected from various sensors. If the degree of redundancy is sufficiently high, the readings from one or more missing sensors can be accurately restored from those remaining healthy sensor readings. By combining an autoencoder [11], [12] with a PSO [13], [14], a MSR algorithm is proposed [11] and extended for designing a robust neuroidentifier [13] and a fault-tolerant linear controller [17]. Fig. 12 shows the structure of a MSR block.

1) Autoencoder: The autoencoder is a multilayer perceptron (MLP) neural network. It is trained to perform an identity mapping, where the network inputs are reproduced at the output layer [see Fig. 12(a)]. The network has the same number of inputs and outputs, but the number of neurons in the hidden layer is less than that of the inputs. This particular structure creates a bottleneck in the feedforward path of the

autoencoder. The dimensionality reduction through the input-to-hidden layer enables the network to extract significant features in data, without restriction on the character of the nonlinearities in the data (nonlinear feature extraction). Hence, the hidden layer captures the correlations between the redundant inputs. On the other hand, the dimensionality expansion through the hidden-to-output layer enables the network to reproduce the high-dimensional inputs at the output layer. In this application, the inputs S, of the autoencoder consist of the vector X, at the present time step as well as at the previous two time steps (i.e., $S(k) = [X(k),\ X(k-1),\ X(k-2)]$). The use of the time-delayed inputs enables the autoencoder to capture the autocorrelations of each sensor data in the vector X.

The autoencoder is firstly trained without any missing sensor. It starts off with small random initial weights. By feeding the data through the autoencoder and adjusting its weight matrices (using backpropagation algorithm), W and V, the autoencoder is trained to map its inputs to its outputs. Once trained, the cross correlations between different sensor data as well as the autocorrelations of each sensor data in the vector X are established by the autoencoder. The detailed training procedure is described in [17].

2) Particle Swarm Optimization (PSO): The PSO [13], [14] is a population based stochastic optimization technique. It searches for the optimal solution from a population of moving particles. Each particle represents a potential solution and has a position (vector x_i) and a velocity (vector v_i) in the problem space. Each particle keeps track of its individual best position $x_{i,\mathrm{pbest}}$, which is associated with the best fitness it has achieved so far, at any step in the solution. Moreover, the best position among all the particles obtained so far in the swarm is kept track of as x_{gbest}. This information is shared by all particles. At each time instant k, a new velocity for particle $i(i = 1, 2, \ldots, N)$ is updated by

$$v_i(k+1) = wv_i(k) + c_1\phi_1(x_{i,\mathrm{pbest}}(k) - x_i(k))$$
$$+ c_2\phi_2(x_{\mathrm{gbest}}(k) - x_i(k)) \qquad (14)$$

where c_1 and c_2 are positive constants representing the weighting of the acceleration terms that guide each particle toward the individual best and the swarm best positions $x_{i,\mathrm{pbest}}$ and x_{gbest}, respectively; ϕ_1 and ϕ_2 are uniformly distributed random numbers in $[0, 1]$; w is a positive inertia weight developed to provide better control between exploration and exploitation; N is the number of particles in the swarm. The last two terms in (14) enable each particle to perform a local search around its individual best position $x_{i,\mathrm{pbest}}$ and the swarm best position x_{gbest}. The first term in (14) enables each particle to perform a global search by exploring a new search space. Based on the updated velocity, each particle changes its position according to the equation

$$x_i(k+1) = x_i(k) + v_i(k+1), \qquad i = 1,\ 2, \ldots,\ N. \quad (15)$$

The final value of x_{gbest} is regarded as the optimal solution of the problem. In this paper, a small population of PSO particles ($N = 5$) is used to reduce the computational cost of the PSO search algorithm. Other parameters for the PSO implementation are chosen as: $c_1 = c_2 = 2.0$, $w = 1.4 - (1.4 - 0.4)\,k/M$, where k is the current iteration number and M is the maximum iteration number.

3) Missing Sensor Restoration: After training the autoencoder, the inputs of the autoencoder are reproduced at its output layer. If one or more sensor measurements are missing, the outputs of the autoencoder $\hat{S}$ no longer match its inputs S, and the error signal E_S becomes significant [see Fig. 12(a)]. In this case, the PSO module in the feedback search loop of the MSR is activated and only the healthy sensor data S_H are fed directly into the autoencoder [see Fig. 12(b)]. The error signal E_S is then used by the PSO as a fitness signal to search for the optimal estimates of the missing sensor data, based on the correlations between the healthy data and the missing data established by the autoencoder. At each iteration, the outputs of the PSO S_M, which represent the estimated missing sensor data, are fed together with the healthy sensor data, through the autoencoder to reduce the value of the following fitness measure function f_i for each particle, defined by

$$f_i = ||E_S|| = ||S_H - \hat{S}_H(S_H, S_M)||, \qquad i = 1, 2, \ldots, N \tag{16}$$

where S_H represents the actual healthy sensor data; $\hat{S}_H$ represents the reproduced healthy sensor data from the autoencoder; S_M represents the estimates of the missing sensor data by the PSO. Once the error is below a predetermined threshold, the output of the autoencoder S_R is regarded as the best estimates of the missing sensor data.

The use of the autoencoder does not need an explicit plant model. In addition, the PSO algorithm provides a fast and efficient search for the optimal solution, because of its attractive features including simple implementation, small computational load, and fast convergence. Therefore, the MSR algorithm is suitable for online application.

C. Design of the SERS

1) Three-Phase Current Sensor Measurements: Power systems normally operate under almost balanced three-phase conditions at the transmission level. Thus, the three-phase currents, i_a, i_b, and i_c, should approximately satisfy the equation

$$i_a + i_b + i_c = 0. \tag{17}$$

Under balanced condition, if the aforementioned relationship conflicts, it indicates that one or more current sensors are lost. A realistic expression for (17) can be written as

$$|i_a + i_b + i_c| < \sigma_1 \tag{18}$$

where σ_1 is a predetermined small threshold value. However, if i_a, i_b, and i_c are all missing, there might be $i_a = i_b = i_c = 0$, and therefore, (18) is satisfied. To distinguish this case from the case of no missing sensor, another equation is used, given by

$$|i_a| < \sigma_2 \quad \text{and} \quad |i_b| < \sigma_2 \quad \text{and} \quad |i_c| < \sigma_2 \tag{19}$$

where σ_2 is a small threshold value. If (18) is satisfied but (19) is not satisfied, there is no sensor missing. Otherwise, one or more current sensors are missing. If only one current sensor is missing, it can be simply restored by using (17). However, in order to
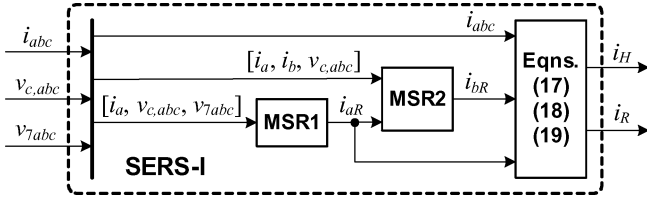
Fig. 13. Structure of the sensor evaluation and (missing sensor) restoration scheme for the three-phase current sensor measurements i_{abc} (SERS-I).

identify and restore multiple missing current sensors, a sensor evaluation and (missing sensor) restoration scheme (SERS-I) is designed, as shown in Fig. 13. A necessary condition for SERS-I implementation is that all the sensor data in $v_{c,abc}$ and v_{7abc} are available. How to determine this condition will be discussed later in the Section V–C3) on the overall structure of the SERS. Here, it is simply assumed that this condition is satisfied. The SERS-I contains two MSR blocks and a block that implements (17)–(19). Each MSR block has the same structure as shown in Fig. 12 and only evaluates the status of one current sensor. If any MSR block determines that the current sensor is missing, its PSO module is activated and only performs a one-dimensional search to restore the missing current. That is, i_a is evaluated and restored by MSR1 if it is missing; i_b is evaluated and restored by MSR2 if it is missing; i_c is calculated by (17) if it is missing. In this application, each MSR converges within 10 iterations to restore one missing sensor measurement. Therefore, the maximum iteration number for the PSO implementation in each MSR block is set at $M = 10$. In addition, a necessary condition for the MSR to work is that the number of healthy inputs must equal or exceed the number of degrees of freedom (DOFs) in the hidden layer. Thus, the dimensions of the input, hidden, and output layers of MSR1 and MSR2 are chosen to be $21 \times 12 \times 21$ and $15 \times 10 \times 15$, respectively. The output vector of the SERS-I, i_R, contains the total restored current sensor data, but i_H contains other healthy current sensor data. These two vectors provide a set of complete current sensor measurements to the SSSC controllers. The implementation procedure of the SERS-I is shown as a flowchart in Fig. 14, where ε_1 and ε_2 are predetermined thresholds for MSR1 and MSR2, respectively. If the error signal, for example, $\|E_{s1}\|$ of MSR1 (see Fig. 12), is smaller than the threshold ε_1, it indicates that i_a, which is monitored by MSR1, is healthy. Otherwise, if $\|E_{s1}\| > \varepsilon_1$, it indicates that i_a is missing and restored by MSR1.

2) DC-Link Voltage Sensor: Under normal operating conditions, the dc-link voltage is almost constant, and its value is far from zero. The following power balance should be held:

$$E = |P_i - P_{\text{loss}}| < \sigma_3 \qquad (20)$$

where P_i is the measured active power injected to the SSSC (Fig. 2); P_{loss} denotes the estimated power loss, including the copper loss, iron loss, switching loss, etc., in the SSSC; and σ_3 is a predetermined threshhold. If (20) is not satisfied, then the measured dc-link voltage is replaced by the nominal value in the SSSC internal controller [18].

3) Overall Structure of the SERS: Fig. 15 shows the overall structure of the SERS. The structure and implementation of the
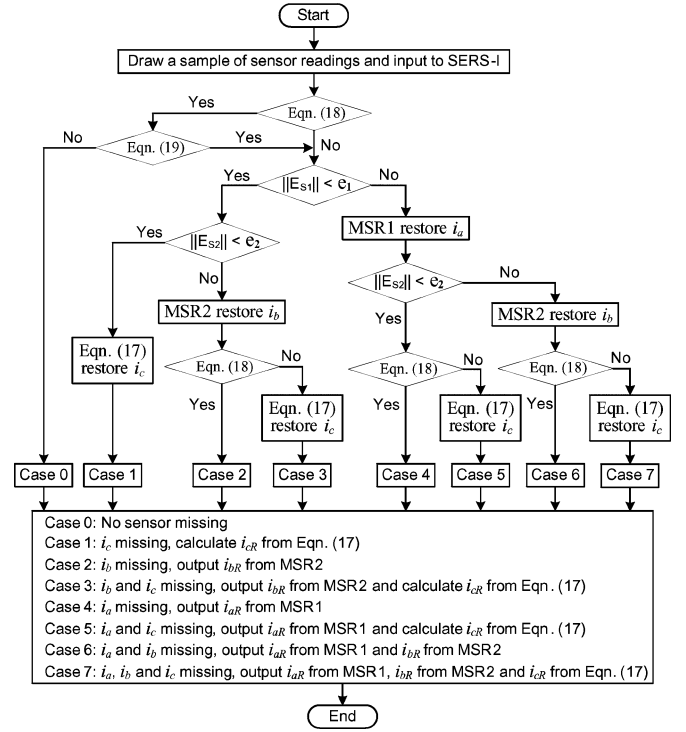

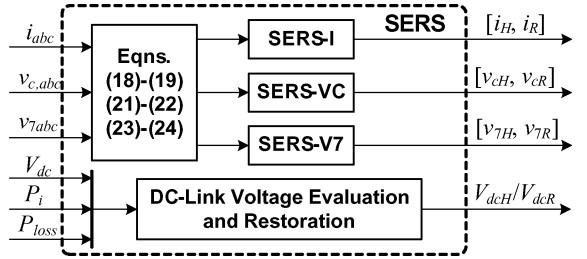Fig. 14. Implementation procedure of the SERS-I.

Fig. 15. Overall structure of the SERS.

SERS-I block have been shown in Figs. 13 and 14, respectively. The SERS-VC and SERS-V7 blocks, which have the same structures as the SERS-I block, are used to evaluate the sensor data and restore the missing sensor data in $v_{c,abc}$ and v_{7abc}, respectively. The status of the sensor data in i_{abc}, $v_{c,abc}$, and v_{7abc} is preevaluated by the equation evaluation block called "Eqns. (18)–(19) (21)–(22) (23)–(24)," where (21)–(24) are given by

$$|v_{ca} + v_{cb} + v_{cc}| < \sigma_4 \qquad (21)$$

$$|v_{ca}| < \sigma_5 \quad \text{and} \quad |v_{cb}| < \sigma_5 \quad \text{and} \quad |v_{cc}| < \sigma_5 \qquad (22)$$

$$|v_{7a} + v_{7b} + v_{7c}| < \sigma_6 \qquad (23)$$

$$|v_{7a}| < \sigma_7 \quad \text{and} \quad |v_{7b}| < \sigma_7 \quad \text{and} \quad |v7c| < \sigma_7 \qquad (24)$$

where σ_4, σ_5, σ_6, and σ_7 are small threshholds. If (21) is satisfied but (22) is not satisfied, there is no sensor missing in $v_{c,abc}$;

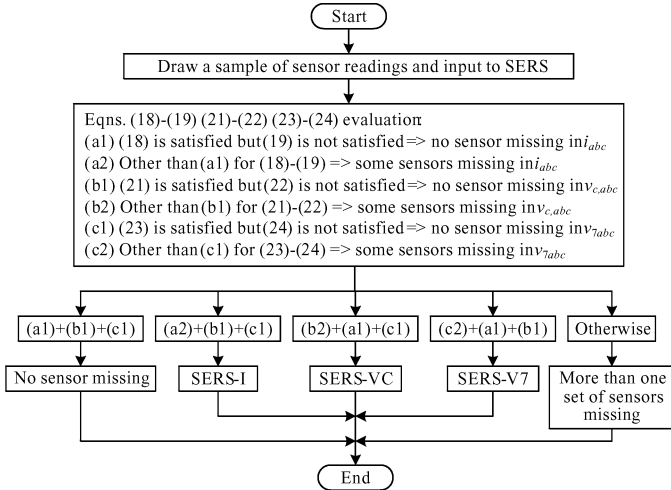Fig. 16. Implementation of the SERS for i_{abc}, $v_{c,abc}$, and v_{7abc}.

Fig. 17. Damping performance of the SSSC controllers during a 150-ms three-phase short circuit at OP-I.

otherwise, one or more sensors in $v_{c,abc}$ are missing. If (23) is satisfied but (24) is not satisfied, there is no sensor missing in v_{7abc}; otherwise, one or more sensors in v_{7abc} are missing. If the equation evaluation block detects that any of the three vectors i_{abc}, $v_{c,abc}$, and v_{7abc} contains missing sensor data, it will activate the corresponding SERS-X (X represents I, VC, or V7) block to identify and restore the missing sensors. This procedure is shown as the flowchart in Fig. 16.

D. Unbalanced Operation

The transmission system of a power network normally operates under a nearly balanced three-phase condition. The unbalanced operations are mainly caused by grid disturbances, such as unbalanced faults including a single-phase-to-ground fault, phase-to-phase fault, etc. Under these conditions, the transmission system experiences a short-term unbalanced operation (e.g., typically 50–200 ms) during the fault, and returns to its balanced three-phase operation after the fault is cleared. During the short-term unbalanced fault, (18), (19), and (21)–(24) will not be applicable to evaluate the status of the sensor data. Therefore, if some sensor data are missing before the unbalanced fault and are still missing when the fault occurs, the signals from the module labeled "Eqns. (18)–(19) (21)–(22) (23)–(24)" in Fig. 15 will be neglected, and the SERS continues to restore the missing sensors during the short-term fault condition. In addition, if three sensor data in one set of sensor measurements, e.g., the three current sensors, are all missing during an unbalanced fault, then the third missing sensor cannot be accurately restored by (17). In this case, one more MSR can be used to restore the third missing sensor data instead of using (17) [17]. However, since the fault only exists for a very short period of time, it will not have any notable effect on the entire system performance. Finally, long-term unbalanced operations rarely happen in the transmission systems. Therefore, they are not considered in the design of the SERS.
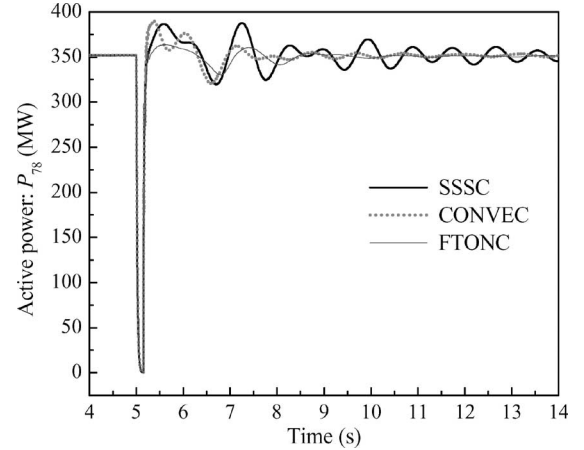
VI. SIMULATION RESULTS

The dynamic performance of the FTONC is evaluated at two different operating points each for three cases: no sensor missing, two current sensors (i_a and i_c) missing, and three current sensors (i_a, i_b, and i_c) missing. In the real system, if some sensors are missing, their values may be read as zeros, some noises, or some uncertain error values. However, the forms of missing sensor readings do not affect the implementation of the SERS. Therefore, during the simulation, the sensor readings are simply set as zeros if they are missing.

A. Test at Operating Point Where Controllers are Designed

The FTONC is trained and the CONVEC is tuned at a specific operating point (called OP-I), where the active power transmitted by line 7–8 is $P_{78} = 352$ MW.

A 150 ms temporary three-phase short circuit is applied in Fig. 1 to the bus 7 end of line 7–8 at $t = 5$ s. Fig. 17 shows the results of P_{78}. The curve SSSC indicates the system response without the external controller applied to the SSSC. These results show that the FTONC has the best power oscillation damping performance compared with the CONVEC and the SSSC, and the CONVEC also improves the damping of the system. However, during the first two swings, the CONVEC is unable to provide effective damping due to the time-delay responses of the two low-pass filters, but the FTONC is already providing damping during this period because it works effectively without the two low-pass filters in the CONVEC.

In order to evaluate the fault-tolerance of the FTONC, two missing sensor tests are applied to the SSSC. The system in Fig. 1 is initially operated under normal conditions. From $t = 8$ s, two current sensors, i_a and i_c, are assumed to be missing, which are detected and restored by the SERS immediately. The restored current sensor data, i_{aR} and i_{cR}, are then used by the SSSC controllers. Fig. 18 compares the values of current components i_d and i_q in the case of no sensor missing and two current sensors missing. These results indicate that with a suitably designed SERS, the missing current sensors are correctly restored. Therefore, the SERS provides a set of fault-tolerant
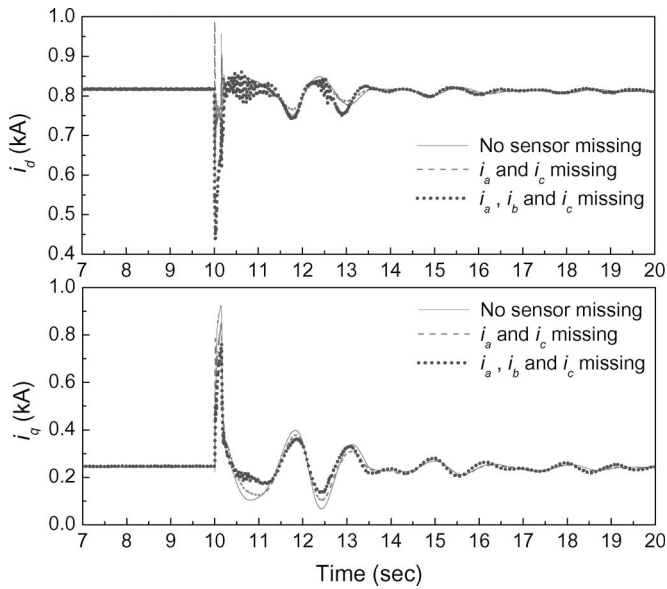
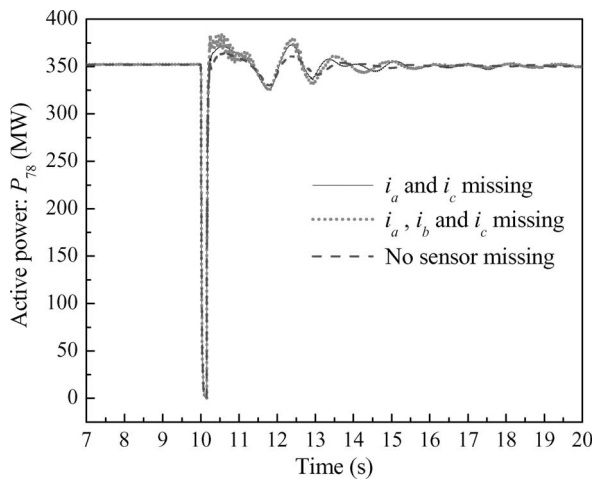Fig. 18.   A 150-ms three-phase short circuit at OP-I: i_d and i_q.

Fig. 19.   Missing sensor tests for the FTONC at OP-I.

complete inputs to the SSSC controllers. As shown in Fig. 19, the FTONC successfully regulate the active power of line 7–8 at the set point value during steady state without any obvious transition at the moment of sensor missing. Thereafter, a 150 ms three-phase short circuit is applied to the bus 7 end of line 7–8 at $t = 10$ s. Compared to the response without any missing sensors, the transient performance of the FTONC degrades slightly due to missing of two current sensors. However, it still provides effective control for the SSSC and efficient power oscillation damping during the transient response after this large disturbance.

In another test, three current sensors, i_a, i_b, and i_c, are all assumed to be missing from $t = 8$ s and restored by the SERS. Thereafter, the same 150 ms three-phase short circuit is applied to the bus 7 end of line 7–8 at $t = 10$ s and the result appears in Figs. 18 and Figs. 19. Compared to the response with two missing sensors, the performance of the SERS degrades when restoring one more missing current sensor, but the SERS is still
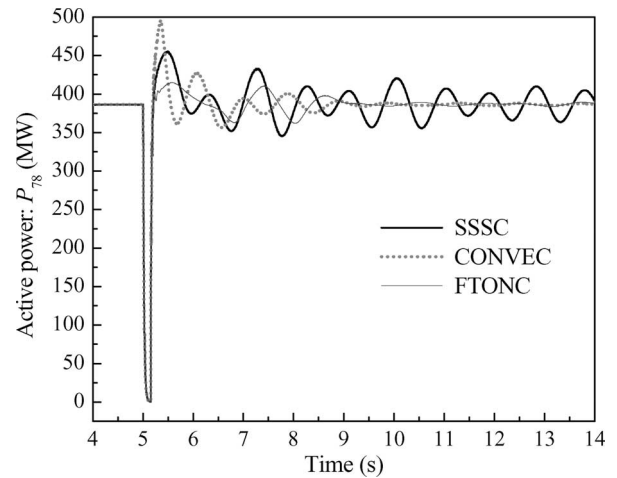

Fig. 20.   Damping performance of the SSSC controllers during a 150-ms three-phase short circuit at OP-II.

able to provide a set of acceptable fault-tolerant inputs to the SSSC controllers. As a result, the transient performance of the FTONC degrades a little further, but it still provides effective control for the SSSC and efficient power oscillation damping even without any required current sensor available during the transient state after this large disturbance.

On the other hand, without the SERS, the SSSC controllers fail to control the SSSC based on the faulty input currents when they are missing. As a result, the SSSC has to be tripped off from the power network.

B. Test at a Different Operating Point

The dynamic performance of the FTONC is now reevaluated at a different operating point (OP-II), where line 4–5 is open during the entire test. This causes a transmission congestion at line 1–6 (i.e., line 1–6 is overloaded) that can be relieved by using the SSSC on line 7–8 [15] to draw more power through line 7–8 (P_{78} increased to 386 MW at OP-II).

The same 150 ms three-phase short circuit is applied to the bus 7 end of line 7–8 at $t = 5$ s. The results of P_{78} are shown in Fig. 20, which again indicates that the FTONC still provides the improved damping performance over the CONVEC at OP-II. The CONVEC is also more efficient than the SSSC.

The same missing sensor and three-phase short circuit tests as in the previous section are applied to the SSSC to evaluate the fault-tolerance of the FTONC. The results of P_{78} are shown in Fig. 21. The FTONC still provides fault-tolerant control for the SSSC and efficient damping at OP-II when two or three crucial current sensor measurements are missing.

C. Test on an Unbalanced Fault at OP-I

In power system transient studies, three-phase short circuits are commonly used to evaluate the system transient performance and stability because they are the most severe faults in the power grid. However in the real power system, most grid faults are unbalanced single-phase-to-ground faults. To further illustrate the robustness of the FTONC, the system is now tested with
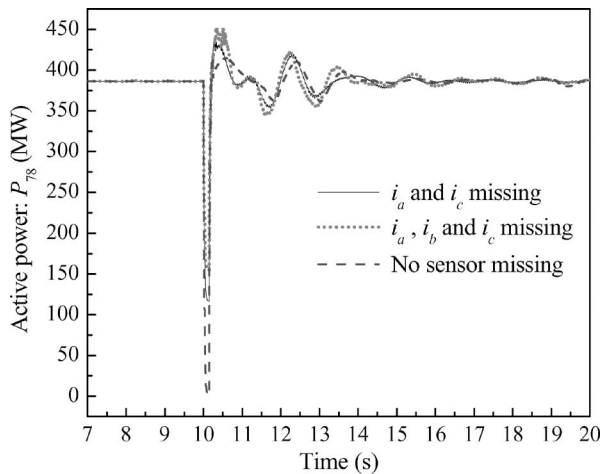
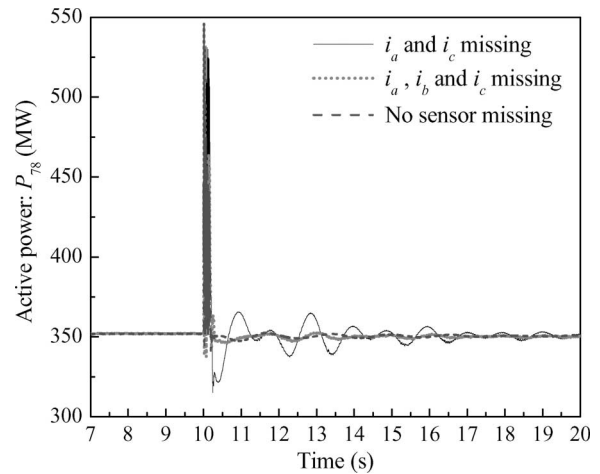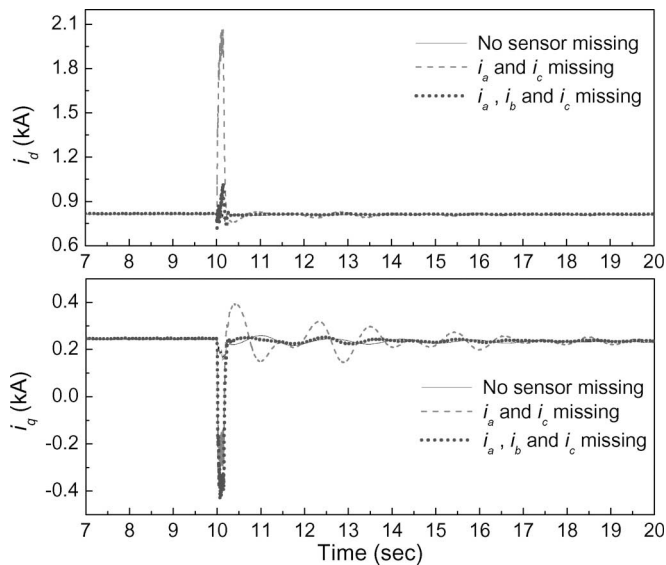Fig. 21.   Missing sensor tests for the FTONC at OP-II.

Fig. 23.   Missing sensor tests for the FTONC at OP-I during a phase-A-to-ground unbalanced fault.

Fig. 22.   A 150-ms phase-A-to-ground fault at OP-I: i_d and i_q.

a phase-A-to-ground fault at OP-I. This unbalanced fault is applied at the bus 7 end of line 7–8 at $t = 10$ s and is cleared after 150 ms. The system experiences an unbalanced operation during the fault, and returns to balanced three-phase operation after the fault is cleared. Two missing sensor tests are applied from $t = 8$ s before the fault: two current sensors i_a and i_c missing, and all three current sensors i_a, i_b, and i_c missing.

Fig. 22 compares the current components i_d and i_q in the case of no sensor missing, two and three current sensors missing; while Fig. 23 shows the corresponding results of P_{78}. This single-phase-to-ground fault causes a larger fault current in phase A than in phases B and C. During the fault, the correlations established by the SERS no longer hold; therefore the performance of the SERS degrades when restoring missing sensors. In contrast to the balanced three-phase faults, this unbalanced fault has more severe effect on the FTONC when two current sensors (including the fault phase A current sensor) are missing;

but it has no notable effect on the FTONC when all three current measurements are missing. Since the fault only exists for a short term, the performance degradation of the SERS does not cause any problem to the SSSC controllers. The FTONC is still able to provide fault-tolerant effective control for the SSSC and efficient damping even when two or three crucial current sensor measurements are missing. These results show that the FTONC is robust to unbalanced faults.

VII. CONCLUSION

An FTONC has been proposed for controlling an SSSC. This FTONC consists of a conventional internal linear controller, an NONC for the external damping control, and an SERS. The DHP technique and RBFNNs are used to design the NONC. The SERS is designed by using the autoassociative neural networks and the PSO. This SERS provides a set of fault-tolerant measurements to the SSSC internal and external controllers, and therefore, guarantees a fault-tolerant control for the SSSC.

Simulation studies have been carried out in the PSCAD/EMTDC environment to implement the FTONC on an SSSC connected to a multimachine power system. Results show that the FTONC provides the expected improved damping performance over the CONVEC used by the SSSC, and a fault-tolerant control to the SSSC even when multiple crucial sensor measurements are missing.

REFERENCES

[1] L. Gyugyi, C. D. Schauder, and K. K. Sen, "Static synchronous series compensator: A solid-state approach to the series compensation of transmission lines," *IEEE Trans. Power Del.*, vol. 12, no. 1, pp. 406–417, Jan. 1997.

[2] B. S. Rigby, N. S. Chonco, and R. G. Harley, "Analysis of a power oscillation damping scheme using a voltage-source inverter," *IEEE Trans. Ind. Appl.*, vol. 38, no. 4, pp. 1105–1113, Jul./Aug. 2002.

[3] J.-W. Park, R. G. Harley, and G. K. Venayagamoorthy, "New external neuro-controller for series capacitive reactance compensator in a power network," *IEEE Trans. Power Syst.*, vol. 19, no. 3, pp. 1462–1472, Aug. 2004.

[4] W. Qiao and R. G. Harley, "Indirect adaptive external neuro-control for a series capacitive reactance compensator based on a voltage source PWM converter in damping power oscillations," *IEEE Trans. Ind. Electron.*, vol. 54, no. 1, pp. 77–85, Feb. 2007.

[5] B. S. Rigby and R. G. Harley, "An improved control scheme for a series-capacitive reactance compensator based on a voltage-source inverter," *IEEE Trans. Ind. Appl.*, vol. 34, no. 2, pp. 355–363, Mar./Apr. 1998.

[6] J.-W. Park, R. G. Harley, and G. K. Venayagamoorthy, "Adaptive-critic-based optimal neurocontrol for synchronous generators in a power system using MLP/RBF neural networks," *IEEE Trans. Ind. Appl.*, vol. 39, no. 5, pp. 1529–1540, Sep./Oct. 2003.

[7] P. J. Werbos, "Approximate dynamic programming for real-time control and neural modeling," in *Handbook of Intelligent Control*, D. White and D. Sofge, Eds.   New York: Van Nostrand Reinhold, 1992, pp. 493–526.

[8] D. V. Prokhorov and D. C. Wunsch, "Adaptive critic designs," *IEEE Trans. Neural Netw.*, vol. 8, no. 5, pp. 997–1007, Sep. 1997.

[9] G. K. Venayagamoorthy, R. G. Harley, and D. C. Wunsch, "Dual heuristic programming excitation neurocontrol for generators in a multimachine power system," *IEEE Trans. Ind. Appl.*, vol. 39, no. 2, pp. 382–394, Mar./Apr. 2003.

[10] R. J. Patton, "Fault-tolerant control: The 1997 situation," in *Proc. IFAC Symp. Fault Detection, Supervision, Safety Tech. Processes (SAFEPROCESS'97)*, Hull, U.K., Aug.1997, pp. 1033–1055.

[11] M. A. El-Skarkawi and Robert J. Marks, II, "Missing sensors restoration for system control and diagnostics," in *Proc. the 4th IEEE Int. Symp. Diagnostics Electric Mach., Power Electron. Drives*, Atlanta, GA, Aug. 24–26, 2003, pp. 338–341.

[12] W. Qiao, Z. Gao, and R. G. Harley, "Continuous on-line identification of nonlinear plants in power systems with missing sensor measurements," in *Proc. 2005 Int. Joint Conf. Neural Netw.*, Montreal, QC, Canada, Jul. 31–Aug. 4, 2005, pp. 1729–1734.

[13] J. Kennedy and R. C. Eberhart, "Particle swarm optimization," in *Proc. 1995 IEEE Int. Conf. Neural Netw.* Nov. 27–Dec. 1, 1995, vol. 4, pp. 1942–1948.

[14] Y. Shi and R. C. Eberhart, "A modified particle swarm optimizer," in *Proc. 1998 IEEE Int. Conf. Evol. Comput.*, Piscataway, NJ, May. 4–9, 1998, pp. 69–73.

[15] S. Jiang, U. D. Annakkage, and A. M. Gole, "A platform for validation of FACTS models," *IEEE Trans. Power Del.*, vol. 21, no. 1, pp. 484–491, Jan. 2006.

[16] S. S. Haykin, *Neural Networks: A Comprehensive Foundation*, 2nd ed. Upper Saddle River, NJ: Prentice-Hall, 1998.

[17] W. Qiao, R. G. Harley, and G. K. Venayagamoorthy, "A fault-tolerant P-Q decoupled control scheme for static synchronous series compensator," in *Proc. the IEEE PES 2006 Gen. Meet.*, Montreal, QC, Canada, Jun. 18–22, 2006, 8 pp.

[18] Y. Jeong, S. K. Sul, S. E. Schulz, and N. R. Patel, "Fault detection and fault-tolerant control of interior permanent-magnet motor drive system for electric vehicle," *IEEE Trans. Ind. Appl.*, vol. 41, no. 1, pp. 46–51, Jan./Feb. 2005.

Ronald G. Harley (M'77–SM'86–F'92) received the M.Sc.Eng. degree (*cum laude*) in electrical engineering from the University of Pretoria, Pretoria, South Africa, in 1965, and the Ph.D. degree in electrical engineering from London University, London, U.K., in 1969.

In 1971, he was appointed to the Chair of Electrical Machines and Power Systems at the University of Natal, Durban, South Africa, where he has been a Professor of electrical engineering, the Department Head, and the Deputy Dean of Engineering. He is currently the Duke Power Company Distinguished Professor at the Georgia Institute of Technology, Atlanta. His current research interests include the dynamic behavior and condition monitoring of electric machines, motor drives, power systems and their components, and controlling them by the use of power electronics and intelligent control algorithms. He is the author or coauthor of about 380 papers in refereed journals and international conferences and three patents.

Prof. Harley is a Fellow of the British Institution of Electrical Engineers (IEE). He is also a Fellow of the Royal Society in South Africa and a Founder Member of the Academy of Science in South Africa formed in 1994. During 2000 and 2001, he was one of the IEEE Industry Applications Society's six Distinguished Lecturers. He was the Vice President of Operations of the IEEE Power Electronics Society (2003–2004) and the Chair of the Atlanta Chapter of the IEEE Power Engineering Society. He is currently the Chair of the Distinguished Lecturers and Regional Speakers Program of the IEEE Industry Applications Society. He is the recipient of the Cyrill Veinott Award in 2005 from the Power Engineering Society for "outstanding contributions to the field of electromechanical energy conversion." Ten of his papers have attracted prizes from journals and conferences.

Ganesh Kumar Venayagamoorthy (S'91–M'97–SM'02) born in Jaffna, Sri Lanka. He received the B.Eng. (Hons.) degree from Abubakar Tafawa Balewa University, Bauchi, Nigeria, in 1994, the M.Sc. (Eng.) degree and the Ph.D. degree in engineering from the University of KwaZulu-Natal (UKZN), Durban, South Africa, in 1999 and 2002, respectively.

He is currently an Associate Professor of electrical and computer engineering and the Director of the Real-Time Power and Intelligent Systems Laboratory, University of Missouri-Rolla (UMR), Rolla. He was a visiting researcher at ABB, Corporate Research, Västerås, Sweden, in 2007. His current research interests include development and applications of computational intelligence for real-world applications including power systems stability and control, flexible ac transmission system (FACTS) devices, alternative sources of energy, sensor networks, and evolvable hardware. He is the author or coauthor of two edited books, three book chapters, 50 refereed journals papers, and 190 refereed international conference proceeding published papers. He has attracted about U.S. $4 million in research funding to date.

Dr. Venayagamoorthy is an Associate Editor of the IEEE TRANSACTIONS ON NEURAL NETWORKS and the IEEE TRANSACTIONS ON INSTRUMENTATION AND MEASUREMENT. He is a Senior Member of the South African Institute of Electrical Engineers (SAIEE). He is also a member of the International Neural Network Society (INNS), the Institution of Engineering and Technology, U.K., and the American Society for Engineering Education. He is currently the IEEE St. Louis Computational Intelligence Society (CIS) and the Industry Applications Society (IAS) Chapter Chairs, the Chair of the Working Group on Intelligent Control Systems, the Secretary of the Intelligent Systems Subcommittee, and the Vice Chair of the Student Meeting Activities Subcommittee of the IEEE Power Engineering Society, and the Chair of the IEEE CIS Task Force on Power System Applications. He is the recipient of the 2007 Office of Naval Research (ONR) Young Investigator Program Award, the 2004 National Science Foundation (NSF) CAREER Award, the 2006 IEEE Power Engineering Society Walter Fee Outstanding Young Engineer Award, the 2006 IEEE St. Louis Section Outstanding Section Member Award, the 2005 IEEE IAS Outstanding Young Member Award, the 2005 SAIEE Young Achievers Award, the 2004 IEEE St. Louis Section Outstanding Young Engineer Award, the 2003 INNS Young Investigator Award, five prize papers from the IEEE IAS and the IEEE CIS, the 2006 UMR School of Engineering Teaching Excellence Award, and the 2005 UMR Faculty Excellence Award. He is listed in the 2008 edition of *Who's Who in the World*. He has organized and chaired several panels, invited and regular sessions, and tutorials at international conferences and workshops.

Wei Qiao (S'05) received the B.Eng. and M.Eng. degrees in electrical engineering from Zhejiang University, Hangzhou, China, in 1997 and 2002, respectively, and the M.S. degree in high-performance computation for engineered systems from Singapore MIT Alliance (SMA), Singapore, in 2003. He is currently working toward the Ph.D. degree at the School of Electrical and Computer Engineering, Georgia Institute of Technology, Atlanta.

From 1997 to 1999, he was an Electrical Engineer in China Petroleum & Chemical Corporation (SINOPEC). His current research interests include power system control and stability, wind energy generation, flexible ac transmission system (FACTS) devices, and the application of computational intelligence in power systems. He is the author or coauthor of over 30 papers in referred journals and international conferences.

Mr. Qiao was the recipient of the first prize in the student paper and poster competition of the IEEE Power Engineering Society General Meeting, Montreal, QC, Canada, in June 2006.